Detecting heavy charged Higgs bosons at the CERN LHC with four *b*-quark tags

D. J. Miller,[1] S. Moretti,[1] D. P. Roy,[2,3,4] and W. J. Stirling[2]
[1]*Rutherford Appleton Laboratory, Chilton, Didcot, Oxon OX11 0QX, United Kingdom*
[2]*Departments of Physics and Mathematical Sciences, University of Durham, South Road, Durham DH1 3LE, United Kingdom*
[3]*Tata Institute of Fundamental Research, Mumbai-400 005, India*
[4]*LAPTH, B.P. 110, F-74941 Annecy-le-Vieux Cedex, France*
(Received 4 June 1999; revised manuscript received 15 September 1999; published 10 February 2000)

We investigate the signature of a heavy charged Higgs boson of the minimal super-symmetric standard model in the lepton plus multijet channel at the CERN Large Hadron Collider with four *b* tags. The signal is the gluon-gluon fusion process $gg \to t\bar{b}H^-$, followed by the $H^- \to \bar{t}b$ decay, while the main background is from $gg \to t\bar{t}b\bar{b}$. We find that the two can be separated effectively by kinematic cuts and mass reconstruction, but the signal size is not very large in the end. Nonetheless, with a good *b*-tagging efficiency $\epsilon_b \sim 50\%$, this channel can provide a viable signature over a limited but interesting range of the parameter space.

PACS number(s): 14.80.Cp, 13.85.−t, 14.65.Fy

I. INTRODUCTION

The detection at the CERN Large Hadron Collider (LHC) of charged Higgs bosons would represent an unequivocal signal of physics beyond the standard model (SM). While the SM predicts only a neutral Higgs boson ϕ, any two-Higgs-doublet extension of it predicts a pair of charged Higgs bosons $H^\pm$ along with three neutral ones: the *CP*-even H and h and the *CP*-odd A [1]. This is true in particular for the minimal supersymmetric extension of the standard model (MSSM). While the SM Higgs boson may be hard to distinguish from one of the neutral Higgs bosons of the MSSM, the charged Higgs boson carries the unambiguous hallmark of the supersymmetric (SUSY) Higgs sector. Moreover, in contrast with the case of super particles, whose signature depends sensitively upon assumptions regarding the *R*-parity status and the nature of the SUSY breaking, the signature of $H^\pm$ bosons is fairly model independent. Therefore, there has been considerable interest in looking for SUSY signals via the associated Higgs sector and in particular the charged Higgs bosons. Furthermore, the masses and couplings of all the MSSM Higgs bosons are given at the tree level in terms of only two parameters: i.e., one of the Higgs boson masses (e.g., M_A) and the ratio of the vacuum expectation values of the two Higgs doublets ($\tan\beta$). Thus the experimental determination of the $H^\pm$ mass $M_{H^\pm}$ would go a long way to quantitatively determining the MSSM Higgs sector.

In the MSSM one has a lower mass limit at the tree level, $M_{H^\pm} > M_{W^\pm}$, which is not significantly modified by radiative corrections. There is also a comparable experimental limit from direct CERN e^+e^- collider LEP2 searches for the charged Higgs boson [2]. In fact, using the MSSM mass relations, one can get a strong indirect bound on $M_{H^\pm}$ in the low-$\tan\beta$ region from the LEP2 limit on M_h, the mass of the lightest Higgs boson of the MSSM [3]. As shown in [4], however, this constraint can be evaded in modest extensions of the MSSM involving an additional singlet Higgs boson. Therefore, it does not preclude direct searches for charged Higgs bosons in the low-$\tan\beta$ region.

The Tevatron and (especially) LHC hadron colliders offer the possibility to carry on the charged Higgs boson search to higher masses because of their higher-energy reach. Here the most prominent source of $H^\pm$ production for $M_{H^\pm} < m_t$ (light charged Higgs boson) is top quark decay, $t \to bH^+$. The corresponding branching ratio (BR) can easily be estimated from the relevant part of the MSSM Lagrangian

$$\mathcal{L} = \frac{e}{\sqrt{2} M_{W^\pm} \sin\theta_W} H^+ (m_b \tan\beta\, \bar{t} b_R + m_t \cot\beta\, \bar{t} b_L), \tag{1}$$

written in the diagonal Cabibbo-Kobayashi-Maskawa (CKM) matrix approximation. It suggests a large $\bar{t}bH^+$ Yukawa coupling and hence a large branching fraction for the $t \to bH^+$ decay in the regions of low as well as very high $\tan\beta$: i.e.,

$$\tan\beta \lesssim 1 \quad \text{and} \quad \tan\beta \gtrsim m_t/m_b\,. \tag{2}$$

Interestingly, these two regions are favored by b-τ unification for a related reason: i.e., assuming $m_b = m_\tau$ at the grand unified theory (GUT) scale, one needs a large $\bar{t}bH^+$ Yukawa coupling contribution to the renormalization group equations (RGEs) to control the rise of m_b at low-energy scales [5]. The dominant decay channels of light charged Higgs bosons are $H^+ \to c\bar{s}$ and $H^+ \to t^* b \to bbW$ at $\tan\beta \lesssim 1$, while the $H^+ \to \tau^+ \nu_\tau$ decay dominates for $\tan\beta > 1$ [6]. It may be noted here that there are already some modest limits on $M_{H^\pm}$ from the Tevatron top quark data [7] in the two regions (2). The search can be extended over a wider region of $M_{H^\pm}$ and $\tan\beta$ at the forthcoming Fermilab Tevatron upgrade (TeV-2), by exploiting the distinctive τ polarization in $H^\pm$ decay [8,9]. Moreover, the detection range can be enlarged to encompass practically the entire $M_{H^\pm} < m_t$ region at the LHC [9,10].

We shall investigate here the prospect of charged Higgs boson searches at the LHC in the opposite case, when $M_{H^\pm} > m_t$ (heavy charged Higgs boson). The dominant decay mode of such a particle is $H^\pm \to t\bar{b}$, which suffers from a large QCD background. Therefore, it is not surprising that detecting a charged Higgs boson heavier than the top quark

has been generally regarded as very hard.[1] The largest signal cross sections at the LHC are expected to come from the associated production of $H^\pm$ with top (anti)quarks, followed by its dominant decay mode, i.e.,

$$gb \to tH^- \to t\bar{t}b \tag{3}$$

and

$$gg \to t\bar{b}H^- \to t\bar{t}b\bar{b}. \tag{4}$$

After the decay of the top quark pair, one expects four b jets in Eq. (4) and three in Eq. (3), where the accompanying $\bar{b}$ sea quark does not take part in the hard scattering and hence escapes detection by being produced close to the beam direction. The charged Higgs signal from Eq. (3) and (4) were investigated in [14] and [15], respectively, assuming triple b tagging. The dominant (QCD) background processes in either case are

$$gg \to t\bar{t}bb, \tag{5}$$

$$gg \to t\bar{t}gg + t\bar{t}q\bar{q}, \tag{6}$$

with one or more of the light parton jets in the latter process misidentified as b. Both analyses found fairly viable $H^\pm$ signals in the two above-mentioned regions of $\tan\beta$, corresponding to a large $H^+\bar{t}b$ Yukawa coupling. Recently, the associated production of charged Higgs and $W^\pm$ bosons has been investigated in [16]. Being a second order electroweak process, however, the size of the resulting signal is smaller than those of reaction (3),(4). Furthermore, it suffers from an overwhelming irreducible background induced by top-quark–top-antiquark production and decay [17]. Therefore, it does not seem to offer a useful $H^\pm$ signal at the LHC. Similarly, the production of charged Higgs scalars in association with b quarks [18] is burdened by a large combinatorial background as well as a formidable multijet QCD noise.

We shall present here an analysis of $H^\pm$ signals at the LHC produced via the gluon-gluon fusion process (4),[2] assuming all four b-quark jets to be tagged. Of course, the size of this signal will be smaller than in the $3b$-tagged channel. However, we have verified, while computing the gg-initiated process, that, by imposing a transverse momentum cut of 20–30 GeV on the spectator b jet in reaction (4), the typical loss of signal is not dramatic: e.g., about a factor of 2–3, for $M_{H^\pm} \approx 300$ GeV. Besides, it is clear from the analyses in Refs. [14,15] that the background (6) with double b mistagging will be very small. Indeed, we have explicitly confirmed this by recomputing the processes (5),(6) from scratch. The same conclusion applies to the the case of single b mistagging in events of the type

$$gb \to t\bar{t}gb. \tag{7}$$

Therefore we only need to worry about the $t\bar{t}b\bar{b}$ background (5). Moreover, we shall see below that the kinematics of the pair of b jets accompanying the $t\bar{t}$ pair is expected to be rather different for the background, as compared to the signal (4). Consequently, such a background can be suppressed effectively by using suitable kinematic cuts on these b jets. As a result, we find a cleaner (but smaller) charged Higgs boson signal in the $4b$-tagged channel than in the $3b$ ones considered in [14,15]. In the following section we present the main steps in the calculation of the signal and background cross sections. The event selection strategy and choice of kinematic cuts are outlined in Sec. III. The quantitative discussion of our analysis is presented in Sec. IV. Finally, we summarize the main results and present our conclusions in Sec. V.

TABLE I. The Y functions for the two independent helicity combinations in terms of the functions S, η, and μ defined in the text. The remaining Y functions can be obtained by flipping the sign of the helicities and exchanging $+$ with $-$ in the S functions and R with L in the chiral coefficients.

$\lambda_1\lambda_2$	$Y(p_1,\lambda_1;p_2,\lambda_2;c_R,c_L)$
$++$	$c_R\mu_1\eta_2 + c_L\mu_2\eta_1$
$+-$	$c_L S(+,p_1,p_2)$

II. CALCULATION OF SIGNAL AND BACKGROUND CROSS SECTIONS

The relatively large number of Feynman diagrams involved in the signal process $gg \to tbH^-$, Eq. (4), renders the algebraic expressions for the corresponding ''squared'' ma-

TABLE II. The Z functions for all independent helicity combinations in terms of the functions S, η, and μ defined in the text. The remaining Z functions can be obtained by flipping the sign of the helicities and exchanging $+$ with $-$ in the S functions and R with L in the chiral coefficients.

$\lambda_1\lambda_2\lambda_3\lambda_4$	$Z(p_1,\lambda_1;p_2,\lambda_2;p_3,\lambda_3;p_4,\lambda_4;c_R,c_L;c'_R,c'_L)$
$++++$	$-2[S(+,p_3,p_1)S(-,p_4,p_2)c'_Rc_R$ $-\mu_1\mu_2\eta_3\eta_4c'_Rc_L - \eta_1\eta_2\mu_3\mu_4c'_L,c_R]$
$+++-$	$-2\eta_2c_R[S(+,p_4,p_1)\mu_3c'_L - S(+,p_3,p_1)\mu_4c'_R]$
$++-+$	$-2\eta_1c_R[S(-,p_2,p_3)\mu_4c'_L - S(-,p_2,p_4)\mu_3c'_R]$
$+-++$	$-2\eta_4c'_R[S(+,p_3,p_1)\mu_2c_R - (S+,p_3,p_2)\mu_1c_L]$
$++--$	$-2[S(+,p_1,p_4)S(-,p_2,p_3)c'_Lc_R$ $-\mu_1\mu_2\eta_3\eta_4c'_Lc_L - \eta_1\eta_2\mu_3\mu_4c'_Rc_R]$
$+-+-$	0
$+--+$	$-2[\mu_1\mu_4\eta_2\eta_3c'_Lc_L + \mu_2\mu_3\eta_1\eta_4c'_Rc_R$ $-\mu_2\mu_4\eta_1\eta_3c'_Lc_R - \mu_1\mu_3\eta_2\eta_4c'_Rc_L]$
$+---$	$-2\eta_3c'_L[S(+,p_2,p_4)\mu_1c_L - S(+,p_1,p_4)\mu_2c_R]$

[1]Recent new insights into the problem can be found in Ref. [11], where the exploitation of top quark polarization effects was advocated. For an alternative approach, using the much suppressed but somewhat cleaner $H^\pm \to \tau\nu$ decay channel, see Ref. [12]. In the same spirit, the mode $H^\pm \to W^\pm h$ is currently being investigated in Ref. [13].

[2]For some early numerical studies of the on-shell $2\to3$ production, see Ref. [19].

trix element rather long and cumbersome. This drawback of the trace method can be obviated by resorting to helicity amplitude techniques, which allow one to write down the ''complex'' amplitudes in more compact form. In expressing the helicity amplitudes, we have made use of the formalism described, e.g., in Ref. [20], to which we refer the reader for technical details. Here we briefly outline the procedure and give all the formulas needed to implement our calculations in a numerical program, as they have not appeared in the literature previously.

First, one needs to introduce some spinor functions Y and Z [21,22,23], given in Tables I and II, which can be defined in terms of the following quantities ($\epsilon^{0123}=1$ is the Levi-Cività tensor):

$$S(+,p_1,p_2)=2\frac{(p_1\cdot k_0)(p_2\cdot k_1)-(p_1\cdot k_1)(p_2\cdot k_0)+i\epsilon_{\mu\nu\rho\sigma}k_0^\mu k_1^\nu p_1^\rho p_2^\rho}{\eta_1\eta_2}, \tag{8}$$

$$S(-,p_1,p_2)=S(+,p_2,p_1)^*,$$

$$\mu_i=\pm\frac{m_i}{\eta_i},\quad \eta_i=\sqrt{2(p_i\cdot k_0)}, \tag{9}$$

where p_i and m_i represent the four-momentum and mass of the particle i (for which $p_i^2=m_i^2$) and k_0 and k_1 are two arbitrary four-vectors such that

$$k_0\cdot k_0=0,\quad k_1\cdot k_1=-1,\quad k_0\cdot k_1=0. \tag{10}$$

In the first of the two expressions in Eq. (9) the signs + and − refer to particles and to antiparticles, respectively.

In Tables I and II the (chiral) coefficients c_R and c_L are those entering the fundamental fermion-fermion-boson vertices, described through the expressions

$$\Gamma^{(\prime)\mu}=\gamma^\mu\Gamma^{(\prime)} \tag{11}$$

and

$$\Gamma^{(\prime)}=c_R^{(\prime)}P_R+c_L^{(\prime)}P_L, \tag{12}$$

with

$$P_R=\frac{1+\gamma_5}{2},\quad P_L=\frac{1-\gamma_5}{2}, \tag{13}$$

the chiral projectors.

If we make the following assignments for the momenta p_i (with $i=1,\ldots,5$), which we assume incoming in the initial state and outgoing in the final state, and helicities. λ_i (with $i=1,\ldots,4$) of the external particles in the $2\to3$ reaction,

$$g(p_1,\lambda_1)+g(p_2,\lambda_2)\to t(p_3,\lambda_3)+\bar{b}(p_4,\lambda_4)+H^-(p_5), \tag{14}$$

so that $p_1^2\equiv p_2^2=0$, $p_3^2=m_t^2$ (with $\Gamma_3=\Gamma_t\neq0$), $p_4^2=m_b^2$ (with $\Gamma_4=\Gamma_b=0$), and $p_5^2=M_{H^\pm}^2$, then the Feynman amplitudes $T_i^{\{\lambda\}}$ can be written (apart from a phase, a factor g_s^2e, and neglecting the color matrices) as (here and below, $\{\lambda\}$ refers cumulatively to the helicities of the external particles λ_i with $i=1,\ldots,4$, and $\Sigma_{\{\lambda\}}$ to the summation over all their possible combinations)

$T_1^{\{\lambda\}}$ = 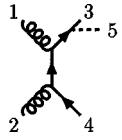 = (15)

$$+N_1N_2D_4(p_3+p_5)D_4(p_2-p_4)$$

$$\times\sum_{i=1,2,4}\sum_{j=2,4}b_ib_j\sum_{\lambda=\pm}\sum_{\lambda'=\pm}$$

$$Y(p_3,\lambda_3;p_i\lambda;c_R^H,c_L^H)$$

$$Z(p_i,\lambda;p_j,\lambda';p_1,\lambda_1,\lambda_1;c_R^g,c_L^g;1,1)$$

$$Z(p_j,\lambda';p_4,-\lambda_4;p_2,\lambda_2;q_2,\lambda_2;c_R^g;c_L^g;1,1),$$

$T_2^{\{\lambda\}}$ = 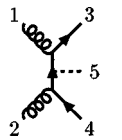 = (16)

$$-N_1N_2D_3(p_3-p_1)D_4(p_2-p_4)$$

$$\times\sum_{i=1,3}\sum_{j=2,4}b_ib_j\sum_{\lambda=\pm}\sum_{\lambda'=\pm}$$

$$Z(p_3,\lambda_3;p_i,\lambda;p_1,\lambda_1;q_1,\lambda_1;c_R^g,c_L^g;1,1)$$

$$Y(p_i,\lambda;p_j,\lambda';c_R^H,c_L^H)$$

$$Z(p_j;\lambda';p_4,-\lambda_4;p_2,\lambda_2;q_2,\lambda_2;c_R^g,c_L^g;1,1),$$

$$T_3^{\{\lambda\}} = \quad = \tag{17}$$

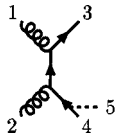

$$+N_1N_2D_3(p_3-p_1)D_3(p_4+p_5)$$

$$\times\sum_{i=i,3}\sum_{j=1,2,3}b_ib_j\sum_{\lambda=\pm}\sum_{\lambda'=\pm}$$

$$Z(p_3,\lambda_3;p_i,\lambda;p_1,\lambda_1;q_1,\lambda_1;c_R^g,c_L^g;1,1)$$

$$Z(p_i,\lambda;p_j,\lambda';p_2\lambda_2;q_2,\lambda_2;c_R^g,c_L^g;1,1)$$

$$Y(p_j,\lambda';p_4,-\lambda_4;c_R^H,c_L^H),$$

$$T_4^{\{\lambda\}} = \quad = T_1^{\{\lambda\}}(1\leftrightarrow 2), \tag{18}$$

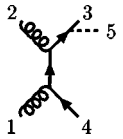

$$T_5^{\{\lambda\}} = \quad = T_2^{\{\lambda\}}(1\leftrightarrow 2), \tag{19}$$

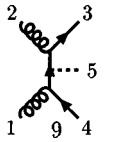

$$T_6^{\{\lambda\}} = \quad = T_3^{\{\lambda\}}(1\leftrightarrow 2), \tag{20}$$

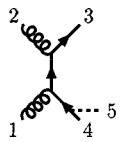

$$T_7^{\{\lambda\}} = \quad = \tag{21}$$

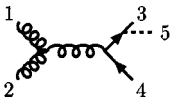

$$+N_1N_2D_4(p_3+p_5)D(p_1+p_2)$$

$$\times\sum_{i=1,2,4}b_i\sum_{\lambda=\pm}\sum_{\lambda'=\pm}$$

$$Y(p_3,\lambda_3;p_i,\lambda;c_R^H,c_L^H)$$

$$[Y(p_i,\lambda;p_1;\lambda';1,1)Y(p_1,\lambda';p_4,-\lambda_4;c_R^g,c_L^g)$$

$$Z(p_1,\lambda_1;q_1,\lambda_1;p_2,\lambda_2;q_2,\lambda;1,1;1,1)$$

$$+2Z(p_2,\lambda_2,q_2,\lambda_2;p_i,\lambda;p_4,-\lambda_4;1,1;c_R^g,c_L^g)$$

$$Y(p_1,\lambda_1;p_2;\lambda';1,1)Y(p_2,\lambda';q_1,\lambda_1;1,1)-\text{same}(1\leftrightarrow 2)],$$

$$T_8^{\{\lambda\}} = \quad = \tag{22}$$

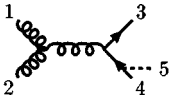

$$-N_1N_2D_3(p_4+p_5)D(p_1+p_2)$$

$$\times\sum_{i=1,2,3}b_i\sum_{\lambda=\pm}\sum_{\lambda'=\pm}$$

$$[Y(p_3,\lambda_3;p_1;\lambda';1,1)Y(p_1,\lambda';p_i,\lambda';p_i\lambda;c_R^g,c_L^g)$$

$$Z(p_1,\lambda_1;q_1,\lambda_1;p_2,\lambda_2;q_2,\lambda_2;1,1;1,1)$$

$$+2Z(p_2,\lambda_2,q_2,\lambda_2;p_3,\lambda_3;p_i,\lambda;1,1;c_R^g,c_L^g)$$

$$Y(p_1,\lambda_1;p_2;\lambda';1,1)Y(p_2,\lambda';q_1,\lambda_1;1,1)-\text{same}(1\leftrightarrow 2)]$$

$$Y(p_i,\lambda;p_4,-\lambda_4;c_R^H,c_L^H),$$

where we have introduced the coefficients $b_1=b_2=-b_3=-b_4=1$, to distinguish incoming and outgoing particles, and the propagators $D_i(p)=1/(p^2-m_i^2+im_i\gamma_i)$ (with $\gamma_i\equiv\Gamma_i$ if $p^2>0$ and $\gamma_i=0$ otherwise[3]) and $D(p)=1/p^2$. In Eqs. (15)–(22), q_i (with $i=1,2$) is an arbitrary four-momentum not parallel to p_i (i.e., $q_i\neq\alpha p_i$ with α constant) and $N_i=[4(q_i-p_i)]^{-1/2}$; see Ref. [20] for more details.

The coefficients c_R and c_L for the vertices relevant to such a process are

$$(c_R^H,c_L^H)=-\frac{1}{\sqrt{2}M_{W^\pm}\sin\theta_W}(m_b\tan\beta,m_t\cot\beta) \tag{23}$$

for the charged Higgs bosons [see Eq. (1)] and simply

$$(c_R^g,c_L^g)=(1,1) \tag{24}$$

for the gluon to quarks couplings. As usual, θ_W represents the Weinberg angle. Here the bottom and top quark masses entering the Yukawa interaction are those defined at the propagator pole, i.e., $m_{b,t}\equiv\overline{m}_{b,t}(m_{b,t})$, where $\overline{m}_{b,t}(Q)$ are the running masses at the (energy) scale Q (see below). Also note that in Eqs. (23), (24) we have factored out the overall couplings $-ie$ and $-ig_s$ of the Lagrangian.

As for the color structure of our process, one should notice that in this case there are two basic combinations of color matrices associated with the Feynman graphs (15)–(22), that is, $(t^At^B)_{i_3i_4}$ and $(t^Bt^A)_{i_3i_4}$, where $A(i_3)$ and $B(i_4)$ identify the colors of the gluons (quarks) 1 (3) and 2 (4), respectively. In fact, it should be recalled that the color terms associated with the triple-gluon vertices are nothing but the structure constants f^{ABX} of the SU(N_C) gauge group, for which

[3]That is, we include a finite quark width only in resonant propagators.

$$[t^A,t^B]_{i_3i_4}\equiv(t^At^B)_{i_3i_4}-(t^Bt^A)_{i_3i_4}=if^{AHX}t^X_{i_3i_4} \qquad (25)$$

X being in our case the color label of the virtual gluon. Therefore, one can conveniently group the original eight Feynman amplitudes as follows:

$$M_+^{\{\lambda\}}=\sum_{i=1}^{3} T_i^{\{\lambda\}}+\sum_{i=7}^{8} T_i^{\{\lambda\}},$$

$$M_-^{\{\lambda\}}=\sum_{i=4}^{6} T_i^{\{\lambda\}}-\sum_{i=7}^{8} T_i^{\{\lambda\}}. \qquad (26)$$

The standard form of the matrix element (ME) squared, summed or averaged over the final or initial spins and colors, is then

$$|\mathcal{M}|^2(gg\to t\bar{b}H^-)=\frac{g_s^4e^2}{256}\sum_{\{\lambda\}}\sum_{i,j=\pm} M_i^{\{\lambda\}}M_j^{\{\lambda\}*}C_{ij}, \qquad (27)$$

where C_{ij} is a 2×2 color matrix with elements

$$C_{++}\equiv C_{--}=\frac{N_C}{4}\left(N_C^2-2+\frac{1}{N_C^2}\right),$$

$$C_{+-}\equiv C_{-+}=\frac{N_C}{4}\left(\frac{1}{N_C^2}-1\right), \qquad (28)$$

$N_C=3$ being the number of colors in QCD. Finally, notice that the ME for the charge conjugated process

$$g(p_1,\lambda_1)+g(p_2,\lambda_2)\to b(p_3,\lambda_3)+\bar{t}(p_4,\lambda_4)+H^+(p_5), \qquad (29)$$

now with $p_3^2=m_b^2$ and $p_4^2=m_t^2$ (and, correspondingly, $\Gamma_3=0$ and $\Gamma_4=\Gamma_t$), can be obtained by the simple replacement $c_R^H\leftrightarrow c_L^H$.

The above formulas refer to the $2\to3$ process of on-shell $H^\pm$ and t production. In reality, both these particles eventually decay inside the detectors, so that one ought also to consider their decay signatures. We have included these decays by convoluting the $2\to3$ (unpolarized) production ME with the three- and one-body decay MEs of top quarks and Higgs bosons, respectively, which are well known and can be found in the literature. In doing so, we introduce several simplifications.[4] First, we neglect spin effects in the top quark decays. Second, we do not consider interference effects between diagrams involving H^+ and H^- production. Third, Fermi-Dirac interference due to the indistinguishibility of b quarks (or, equivalently, of b antiquarks) in the final state are not included. However, while noticeably simplifying the numerical evaluation, we have checked that these approximations do not spoil the validity of our analysis. In fact, we have also produced the exact $2\to8$ ME for the signal process, including all the above spin and interference effects, by means of the HELAS [24] subroutines and the MADGRAPH [25] package, and compared its yield to that of the simplified implementation. We have always found good agreement between the two, with residual effects surviving only in differential spectra which are of no concern in our analysis. Indeed, for the typical quantities we shall investigate (transverse momenta, pseudorapidity, multi jet invariant masses, etc.), the results generally coincide within numerical accuracy.

The HELAS libraries and MADGRAPH have also been used to generate the background process (5), as any analytical expression for the latter would be much too cumbersome. Indeed, 36 different Feynman diagrams are involved (actually twice that if one considers also those induced by the above-mentioned Fermi-Dirac statistics), with 10 external particles.

Both signal and background MEs have been integrated by means of VEGAS [26], with a careful mapping of the phase space, to account for the various resonances. In some cases, where the multidimensional integrations (21 in total, for the $2\to8$ implementation) are more problematic, the VEGAS results have been cross-checked against those obtained by using RAMBO [27] as well as the D01GCF and D01GZF NAGLIB subroutines.

In addition to the phase space integration, one also has to convolute in the (x,Q^2)-dependent parton distribution functions (PDFs) for the the two incoming gluons. These have been evaluated at leading order, by means of the Martin-Roberts-Stirling (MRS) leading order (LO) packages (05A, 09A, 10A, 01A, 07A) [28]. The Q^2 used for the latter was the c.m. energy (squared) at the parton level, i.e., $\hat{s}=x_1x_2s$, with $\sqrt{s}=14\,\mathrm{TeV}$ taken as the c.m. energy for the LHC. The same choice has been adopted for the scale of the strong coupling constant α_s, evaluated again at lowest order, with $\Lambda_{\mathrm{QCD}}^{N_f=4}$ chosen in accordance with that of the PDF set used.

In addition, notice that before the signal and background cross sections can be computed reliably, one must take into account the effects of higher-order QCD corrections to the tree-level processes (see the discussion in Ref. [15]). The full next-to-leading order corrections are as yet unknown for the processes we consider. For the case of the Higgs signal, the dominant effects can, however, be mimicked by adopting the pole masses in the Higgs-boson-fermion coupling entering the production process [see Eq. (23)], rather than the running ones [29]. As for the $t\bar{t}b\bar{b}$ background, we estimate their effect by including an overall K factor of 1.5 throughout this study [15].

The numerical values of the SM parameters are (pole masses are assumed)

$$m_l=m_{\nu_l}=m_u=m_d=m_s=m_c=0,$$

$$m_b=4.25\,\mathrm{GeV},\quad m_l=175\,\mathrm{GeV},$$

$$M_z=91.19\,\mathrm{GeV},\quad \Gamma_z=2.5\,\mathrm{GeV},$$

[4]Note that in the numerical simulations we allow the top quark and Higgs bosons to be ''off shell,'' that is $p_{3[4]}^2\neq m_t^2$ and $p_5^2\neq M_{H^\pm}^2$ in the above formulas for process (14) [29].

$$M_{W^\pm}=80.23\,\text{GeV}, \quad \Gamma_W=2.08\,\text{GeV}. \tag{30}$$

For the top quark width Γ_t, we have used the LO value calculated within the MSSM (i.e., $\Gamma_t=1.55\,\text{GeV}$ for $M_{H^\pm} \gg m_t$). Furthermore, we have adopted M_A and $\tan\beta$ as independent input parameters defining the Higgs sector of the MSSM at LO. The charged Higgs boson width $\Gamma_{H^\pm}$ has been computed by means of the program HDECAY, which indeed requires M_A, rather than $M_{H^\pm}$, as mass input [30] (the masses of the superpartners of the ordinary matter particles were fixed well above 1 TeV, so they enter neither the top quark nor the charged Higgs boson decay chain as real objects and render the virtual SUSY corrections to the $H^\pm tb$ decay vertex negligible [31]). As this program uses running quark masses (in the modified minimal subtraction scheme) in evaluating the decay width of the $H^\pm \to tb$ channel, we have, for consistency, used running values for all such quantities in the $H^\pm tb$ couplings entering our decay MEs for the signal [but not in the propagators and in the phase space, for which the pole masses $m_b \equiv \overline{m}_b(m_b)$ and $m_t \equiv \overline{m}_t(m_t)$ of Eq. (30) have been used].

Finally, notice that we stop our analyses at the parton level, without considering fragmentation and hadronization effects. Thus jets are identified with the partons from which they originate and all cuts are applied directly to the latter. In particular, when selecting b jets, a vertex tagging is implied, with finite efficiency ϵ_b per tag. As four b jets will be required to be tagged, the overall efficiency will be c_b^4, by which both signal and background rates will eventually have to be multiplied. For simplicity, we assume no correlations between the four tags: nor do we include misidentification of light-quark (including c-quark) jets produced in the $W^\pm$ decay as b jets.

III. SELECTION STRATEGY

In this section we describe the kinematic procedure adopted to disentangle charged Higgs events (4) from the background (5) in the $t\bar{t}b\bar{b}$ channel. First, one of the top quarks is required to decay leptonically ($t \to bl\nu$) to provide a hard lepton ($l=e,\mu$) trigger and avoid the QCD background, while the other decays hadronically ($\bar{t} \to \bar{b}qq'$), with $(q,q' \neq b,t)$. The resulting branching fraction is $2 \times 2/9 \times 2/3$, with the factor of 2 accounting for the fact that each of the $W^\pm$'s can decay either leptonically or hadronically. We assume that the charge of the b jet is not measured. Thus the signature we are discussing is effectively

$$4b + 2\ \text{jets} + l^\pm + p^\tau_{\text{miss}}, \tag{31}$$

where the two untagged jets and the $l + p^T_{\text{miss}}\ (=p^T_\nu)$ arise from the W^+W^- boson pair produced in the $t\bar{t}$ decay.

We note that all the decay products of the top quarks in the signal are expected to be hard, while one of the accompanying b quarks (or both depending on the $M_{H^\pm}-m_t$ mass difference) could be soft. Therefore, we impose a relatively demanding transverse momentum cut on the two softer b jets:

$$p^T_{b_1,b_2} > 20\ \text{GeV}. \tag{32}$$

For simplicity, we do the same for the rest, i.e.,

$$p^T_{l^\pm,\nu_1,j,b_3,b_4} > 20\ \text{GeV}. \tag{33}$$

However, we will present some results also for the case of a 30 GeV cut in transverse momentum (on both jets and leptons), since the latter threshold is believed optimal in increasing the b-tagging efficiency at high luminosity (this is needed in order to render the $4b$ signal of a charged Higgs boson statistically significant): see Ref. [32]. Furthermore, we require the pseudorapidity of jets and leptons to be

$$|\eta_{b,j,l^\pm}| < 2.5, \tag{34}$$

and allow for their detection as separate objects by imposing the following isolation criteria:

$$\Delta R_{bb,bj,jj,bl^\pm,jl^\pm} > 0.4, \tag{35}$$

by means of the variable

$$\Delta R_{ij} = \sqrt{(\Delta\eta_{ij})^2 + (\Delta\phi_{ij})^2}, \tag{36}$$

defined in terms of relative differences in pseudorapidity η_{ij} and azimuth ϕ_{ij}, with $i \neq j = j,b,l^\pm$.

We simulate calorimeter resolution by a Gaussian smearing of p^T (without shower spreading and with uniform pseudorapidity and azimuth segmentation), with $[\sigma(p^T)/p^T]^2 = (0.6/\sqrt{p^T})^2 + (0.04)^2$ for all the jets and $[\sigma(p^T)/p^T]^2 = (0.12/\sqrt{p^T})^2 + (0.01)^2$ for the leptons [14]. The corresponding p^T_{miss} is evaluated from the vector sum of the jet and lepton transverse momenta after resolution smearing.

To improve the signal/background ratio and to estimate the $H^\pm$ mass, we follow a strategy similar to the one in Ref. [14].

(a) The invariant mass of the two untagged jets is required to be consistent with $M_{W^\pm}$,

$$|M_{jj} - M_{W^\pm}| \leqslant 15\ \text{GeV}. \tag{37}$$

(b) The neutrino momentum is reconstructed by equating $p^T_\nu = p^T_{\text{miss}}$ and fixing the longitudinal component p^L_ν via the invariant mass constraint $M(l\nu) = M_{W^\pm}$. The latter gives two solutions. If they are complex, we discard the imaginary parts and they coalesce; otherwise, both the solutions are retained.

(c) The invariant mass formed by combining the untagged jet pair with one of the four b jets is required to match m_t:

$$|M_{jjb} - m_t| \leqslant 25\ \text{GeV}. \tag{38}$$

If several b jets satisfy this constraint, the one giving the best agreement with m_t is selected.

(d) The invariant mass formed by combining l and ν with one of the three remaining b jets is also required to match m_t within ± 25 GeV. If several b jets satisfy this, the one giving the best agreement with m_t is selected along with the corresponding value of p^L_ν.

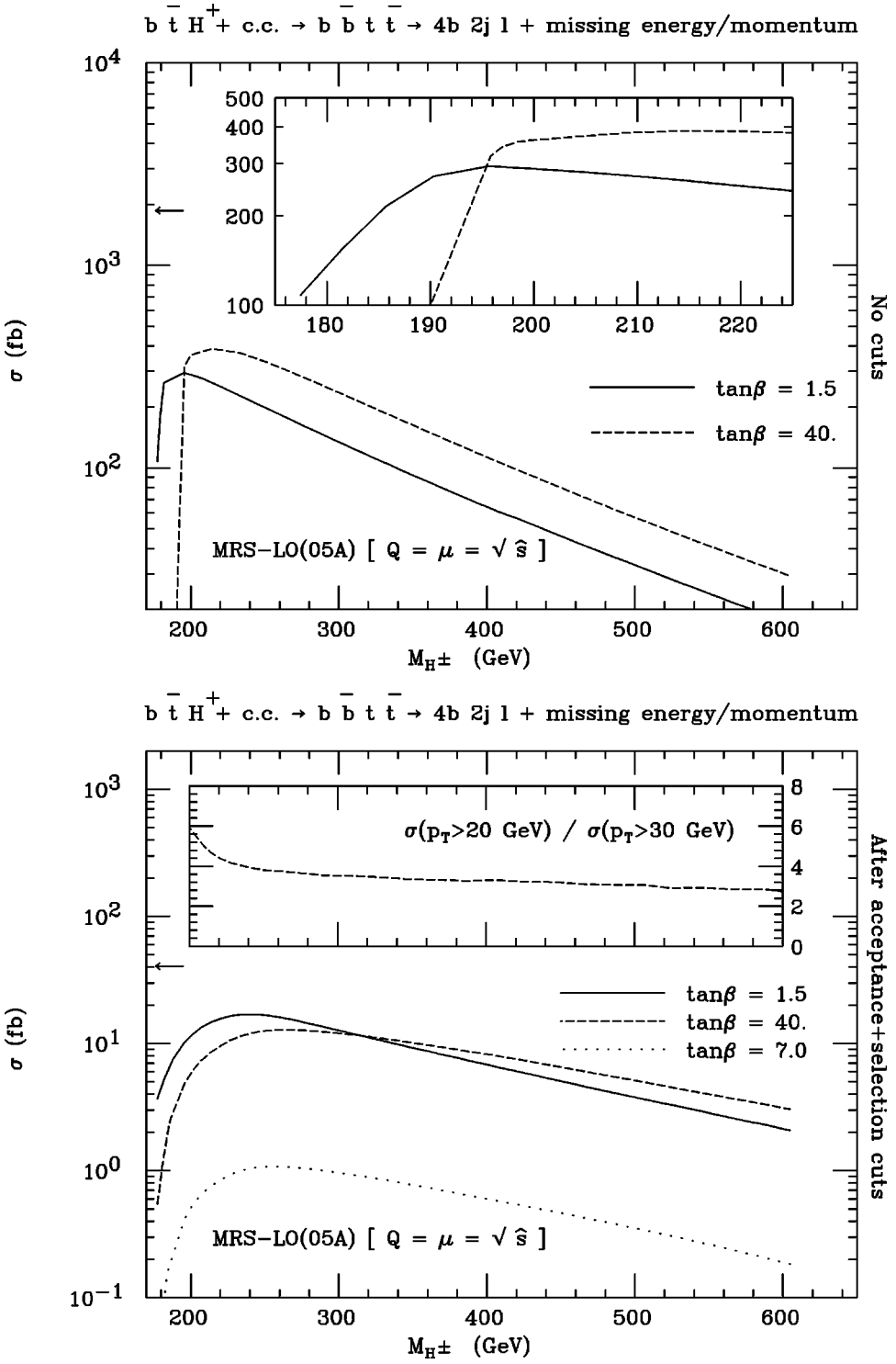

FIG. 1. Production cross section for process (4) (and its charge conjugate) in the decay channel (31) as a function of $M_{H^\pm}$ in the heavy mass range, for some discrete values of $\tan\beta$, for the case in which no (upper figure) and acceptance plus selection (lower figure) cuts have been implemented. In the inset of the upper plot, we enlarge the rates in the vicinity of $M_{H^\pm}=m_t$. In the inset of the lower plot, we present the ratio between the above signal cross section for $\tan\beta=40$ and the corresponding one obtained by adopting a threshold of 30 GeV in (32), (33). The PDF set used was MRS-LO (05A) with renormalization and factorization scales set equal to the partonic c.m. energy. The arrow represents the size of the background (5) yielding the same signature (31). No *b*-tagging efficiency is included.

(e) The remaining pair of *b* jets may be looked upon as the *bb* pair accompanying the *tt* in the signal (4) and background (5). Note that one of these *b* jets is expected to come from the $H^\pm$ decay in the signal, while for the background they both come from a gluon splitting. Consequently, in the latter case one supposes the $b\bar{b}$ pair to have a smaller invariant mass. Furthermore, one may also expect the energy and relative angle of the two *b*'s to be rather different, between signal and background. We compare the signal and background cross sections against M_{bb}, E_{b_1}, E_{b_2} [with the labels 1 (2) referring to the more (less) energetic of the two *b* quarks] and $\cos\theta_{bb}$ and suppress the latter by suitable cuts in one or more such quantities.

(f) Finally, we combine each of the reconstructed *t* quarks with each of the remaining *b* jets to obtain four entries for the *bt* invariant mass M_{bt}. For each signal point, one of these entries will correspond to the parent $H^\pm$ mass, while the other three will represent the combinatorial background.

TABLE III. Production cross section for the signal (4) (and its charge conjugate) in the decay channel (31) (top), for $\tan\beta=30$ and five values of $M_{A(H^\pm)}$ (given in GeV) in the heavy mass range, as obtained by using five different sets of PDFs. Corresponding rates for the backgrond (5) yielding the same signature (31) are also given. No cuts have been implemented. The renormalization and factorization scales are set equal to the partonic z.m. energy. Errors are as given by VEGAS.

			Signal, $\tan\beta=30$ (fb)		
$M_{A(H^\pm)}$	05*A*	09*A*	10*A*	01*A*	07*A*
200(214)	217.14 ± 0.18	226.67 ± 20	199.11 ± 0.15	204.48 ± 0.17	222.79 ± 0.18
300(310)	123.20 ± 0.10	130.79 ± 0.11	110.90 ± 0.086	116.42 ± 0.10	125.76 ± 0.11
400(407)	60.414 ± 0.059	65.256 ± 0.066	53.410 ± 0.049	57.333 ± 0.057	61.360 ± 0.059
500(506)	30.802 ± 0.044	33.895 ± 0.047	26.742 ± 0.040	29.481 ± 0.043	31.252 ± 0.045
600(605)	16.341 ± 0.029	18.268 ± 0.032	13.977 ± 0.026	15.670 ± 0.029	16.455 ± 0.029
			Background (fb)		
	05*A*	09*A*	10*A*	01*A*	07*A*
	1863 ± 56	1949 ± 59	1706 ± 51	1755 ± 53	1901 ± 57
			MRS-LO $[Q=\mu=\sqrt{\hat{s}}]$		
	$4b+2$ jets$+l^\pm+p^T_{\rm miss}$				No cuts

We plot the signal and background cross sections against this quantity. The former will show the resonant peak at $M_{H^\pm}$ sitting on top of a broad combinatorial background, while the latter will show only a broad distribution in M_{bt}. As we shall see below, the Breit-Wigner peak itself can help to improve the signal/background ratio further as well as to determine the $H^\pm$ mass.

(g) For $M_{H^\pm}\gg m_t$, one of the above-mentioned b jets (i.e., the one coming from the $H^+\to t\bar{b}$ decay) would generally be much harder than the other. In this case, one can expect to reduce the combinatorial background by combining each of the top quark pairs with the harder of the two accompanying b jets. This would give two values of the invariant mass M_{bt} for each signal point, one of which corresponds to the parent $H^\pm$ mass. Therefore, we shall also show the signal and background cross sections against this quantity for $M_{H^\pm}\geqslant 300$ GeV.

IV. RESULTS AND DISCUSSION

Both signal (4) and background (5) cross sections are finite over the entire phase space, provided the b-quark mass is retained in the calculation. Thus, as a preliminary exercise, we look at the total production rates of the above processes with no cuts whatsoever, as they would appear in the decay channel (31) to an ideal detector. This is done in the top plot of Fig. 1. Here, the rates have been obtained by multiplying the $2\to3$ cross section times the relevant BRs of quark and Higgs boson decays, thus neglecting finite width effects. The signal rates depend on both $M_{H^\pm}$ and $\tan\beta$, and so they are plotted as a function of the former for two values of the latter in the favorable regions (2). In contrast, the background rates are independent of both and are indicated by the arrow next to the y axis. The inset in the top plot of Fig. 1 enlarges the region around the threshold region $M_{H^\pm}\approx m_t$, where the $\mathcal{B}(H^+\to t\bar{b})$ increases rapidly. A striking feature of the production cross sections is the apparently poor signal-to-background ratio, over all the $M_{H^\pm}$ spectrum considered, irrespective of $\tan\beta$. Note, however, that no dedicated treatment of the final state kinematics has yet been performed. Indeed, the number of heavy charged Higgs events produced is sizable up to around 800 GeV, where the total cross section at both $\tan\beta$ values is still around several femtobarns. At its maximum, just after the opening of the $H^+\to tb$ decay threshold, it can be larger by about two orders of magnitude.

Figure 1 has been produced by using the MRS-LO(05A) PDF set. In Table III we study the dependence of both signal and background rates on the choice of the structure functions, using the other four fits of the 1998 Martin-Roberts-Stirling-Thorne LO package.[5] For reference, we have used the value $\tan\beta=30$, whereas five different choices of Higgs boson masses in the heavy range have been adopted. Differences in the signal cross sections are found to be within the $\pm25\%$ range, with a somewhat smaller range for the background. Furthermore, changing the renormalization (Q) and factorization (μ) scales from their common default value $\sqrt{\hat{s}}$ to, e.g., the sum of the rest masses in the $2\to3$ and $2\to4$ production process (4) and (5), induces variations in the results of the same order as above. As a consequence, an overall error of, say, approximately 30–35 % should be taken as an estimate of the uncertainties related to the PDFs and α_s throughout the paper.

As the next step of our analysis, we implement the acceptance cuts (32)–(35) and the selection cuts described through steps (a)–(d) in the previous section. The total signal and background cross sections after such constraints have been enforced can be found in the bottom plot of Fig. 1. Note that the kinematic procedure outlined above has been helpful in

[5]The additional fits correspond to varying the large-x gluon and α_s about their central preferred values.

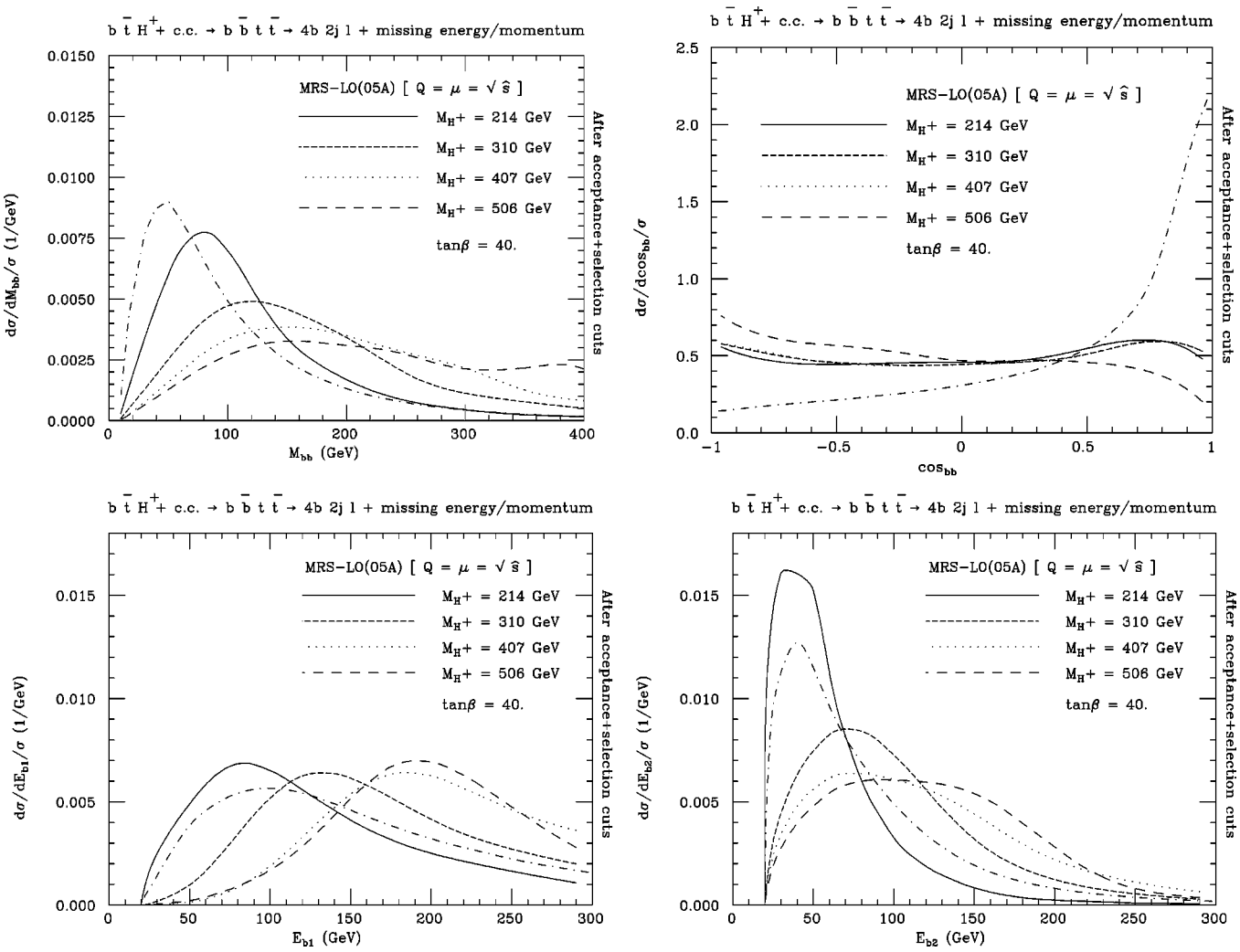

FIG. 2. Differential distributions in invariant mass (top-left), in cosine of the relative angle (top-right) and in energy of the most (bottom-left) and least (bottom-right) energetic of the two b quarks accompanying the $t\bar{t}$ pair, for process (4) (and its charge conjugate) in the decay channel (31), for four selected values of $M_{H^\pm}$ in the heavy mass range, with $\tan\beta=40$. Acceptance and selection cuts have been implemented here. The PDF set used was MRS-LO(05A) with renormalization and factorization scales set equal to the partonic c.m. energy. The fifth (dot-dashed) curve represents the shape of the background (5) yielding the same signature (31). All distributions are normalized to unity. No b-tagging efficiency is included.

increasing the signal-to-background ratio over all the Higgs boson mass spectrum (compare to the curves above). The signal rates have been depleted too, mainly by the $p_{b_2}^T$ cut (32), dropping to a few femtobarns for values of $\tan\beta$ at the upper and lower ends of the parameter range and Higgs boson masses below 700 GeV or so. For intermediate values of $\tan\beta$, e.g., around the minimum of the production cross section occurring at $\tan\beta\approx 7$, prospects are more gloomy. In fact, the signal rates are always below 1 fb or so in this case, for any $M_{H^\pm}$ value. Furthermore, as here (and in the following as well) we have retained a finite value for Γ_H, the reader may appreciate—by comparing this plot to the one above—the suppressing (enhancing) effects of a larger (smaller) Higgs width at low (high) $M_{H^\pm}$ values for $\tan\beta=40$, with respect to the case $\tan\beta=1.5$ (the effects of a $\Gamma_t\neq 0$ are the same in all cases). As intimated in the previous section, we also have considered the case of a 30 GeV cut in all transverse momenta (including the missing one). The inset in the bottom plot of Fig. 1 presents the consequent suppression on the signal rates for, e.g., $\tan\beta=40$. Far from the $M_{H^\pm}\approx m_t+m_b$ threshold, the ratio between the two cross sections stabilizes at just below 3 (irrespectively of $\tan\beta$). For the background, the reduction is slightly higher, a factor of 4 or so.

Continuing with step (e) of our plan, we next investigate the mass, angular, and energy behaviors of the two b quarks accompanying the $t\bar{t}$ pair, after the acceptance and selection cuts have been implemented. The relevant plots can be found in Fig. 2. For reference, the value chosen for $\tan\beta$ is 40, whereas for the charged Higgs boson masses we have taken $M_{H^\pm}=214(310)[407]\{506\}$ GeV, corresponding to $M_A=200(300)[400]\{500\}$ GeV. (Spectra look rather similar if a $p_{l^\pm,\nu j}^T, b>30$ GeV cut is enforced instead.) As already foreseen, one can appreciate significant differences

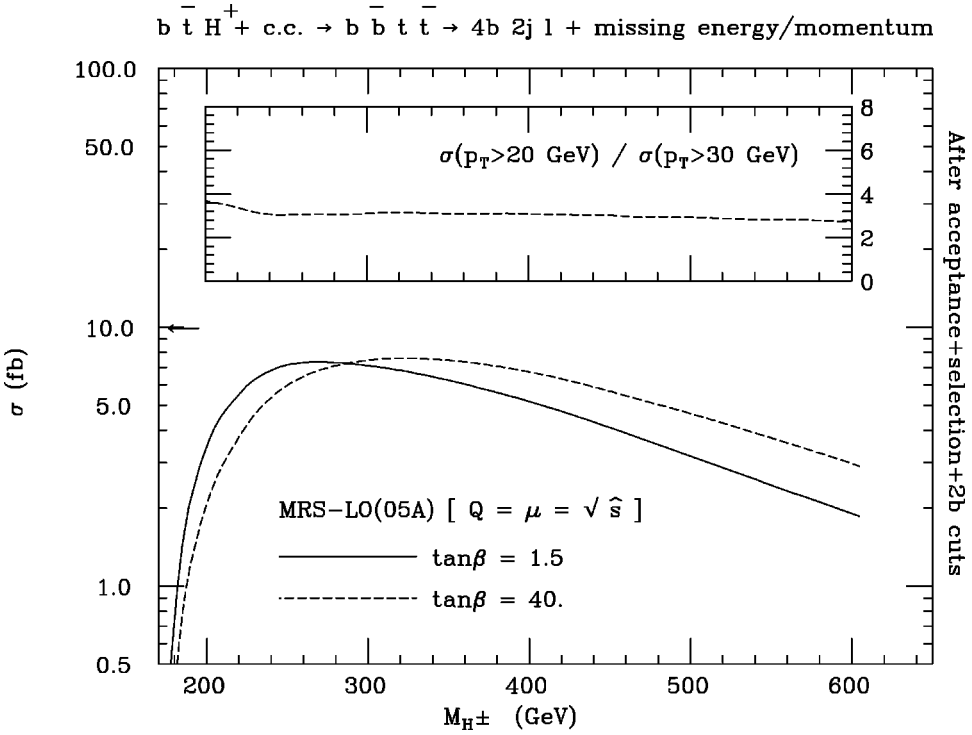

FIG. 3. Production cross section for process (4) (and its charge conjugate) in the decay channel (31) as a function of $M_{H^\pm}$ in the heavy mass range, for two discrete values of $\tan\beta$. Acceptance and selection cuts have been implemented here, along with the additional cuts (39) on the $2b$ system accompanying the $t\bar{t}$ pair. In the inset, we present the ratio between the above signal cross section for $\tan\beta=40$ and the corresponding one obtained by adopting a threshold of 30 GeV in (32),(33). The PDF set used was MRS-LO(05A) with renormalization and factorization scales set equal to the partonic c.m. energy. The arrow represents the size of the background (5) yielding the same signature (31). No b-tagging efficiency is included.

in all four quantities considered, as long as $M_{H^\pm}$ is well above m_t. If $M_{H^\pm}$ is not much larger than 200 GeV, the signal and background distributions are similar except for the angular variable. In contrast, if $M_{H^\pm}\gtrsim 300\,\text{GeV}$, one can see a greater discriminatory power in each of these variables.

In order to enhance the signal-to-background ratio, especially in the very heavy Higgs boson mass region, we therefore adopt the following additional constraints on the two-b-jet system:

$$M_{bb}>120\ \text{GeV}, \quad \cos\theta_{bb}<0.75, \quad E_{b_1}>120\ \text{GeV}. \tag{39}$$

The resulting signal cross sections are shown in Fig. 3 for $\tan\beta=1.5$ and 40 along with those of the background. The signal-to-background ratio has increased, but the background remains larger. However, notice the very little loss of signal at very large Higgs boson masses. In fact, the Higgs rates remain above 1 fb for $M_{H^\pm}\lesssim 800$ GeV. For a transverse momentum cut of 30 GeV throughout, the typical suppression on the signal (away from threshold) is again about a factor of 3 (see the inset in the figure), now similar to the case of the background.

To enhance the relative rates further and estimate the charged Higgs boson mass, we reconstruct the M_{bt} invariant mass by combining each of the reconstructed top quarks with each of the accompanying b jets, as described in step (f), a quantity that we label $M_4(H)$. The resulting spectra are presented in the top plot of Fig. 4 for $\tan\beta=40$ and six selected values of the $H^\pm$ mass along with the background. The signal distribution clearly shows a resonance at $M_4(H)\approx M_{H^\pm}$ sitting over a combinatorial continuum, while the background spectrum is broader and tends to concentrate at values of $M_4(H)$ below 300 GeV. One can sharpen the resonances at the cost of reducing the size of the signal by combining each of the reconstructed t quarks with the harder b jet, as in step (g) [the corresponding invariant mass is labeled as $M_2(H)$]. The distributions that we obtain in this way are given in the bottom part of Fig. 4.

One sees from the figure that the signal-to-background ratio is (much) greater than 1 in the neighborhood of the resonant peaks. This is an advantage of the $4b$-tagged channel over the $3b$-tagged case considered in Ref. [14], where the backgrounds were found to exceed the signal. In contrast, the size of the Higgs cross section is smaller in our case, because of the kinematic suppression induced by requiring the detection of the fourth b quark. However, with an annual luminosity of 100 fb^{-1}, expected from the high-luminosity option of the LHC, and a very good b-tagging efficiency, one would obtain a clearly viable signal. To illustrate this we show the signal rates on the right-hand scale of Fig. 4, for an optimistic b-tagging factor of $\epsilon_b^4=0.1$, corresponding to $\epsilon_b=56\%$. Such a high value is now considered realistic for the TeV-2 run at Fermilab and can be achieved by combining the silicon vertex and the lepton tagging efficiencies [33]. It is also close to the optimistic expectation of a b-tagging efficiency of about 50% even for the high luminosity run of the LHC [32].

For the above efficiency and luminosity, one would obtain between 10 and 100 Higgs events per year with signal-to-background ratios above 1 for $M_H^\pm$ as large as 800 GeV (for $\tan\beta=40$), as shown in Table IV. This shows the predicted number of events in a window of 80 GeV centered around the Higgs resonances for both signal and background, together with the corresponding statistical factors $S/\sqrt{B}$. By looking at those rates, one would expect an accessible signal for $M_{H^\pm}\lesssim 600$ GeV in the high-tan β region ($\gtrsim 40$). Similar results also hold for the case of low-tan β values ($\lesssim 1.5$).

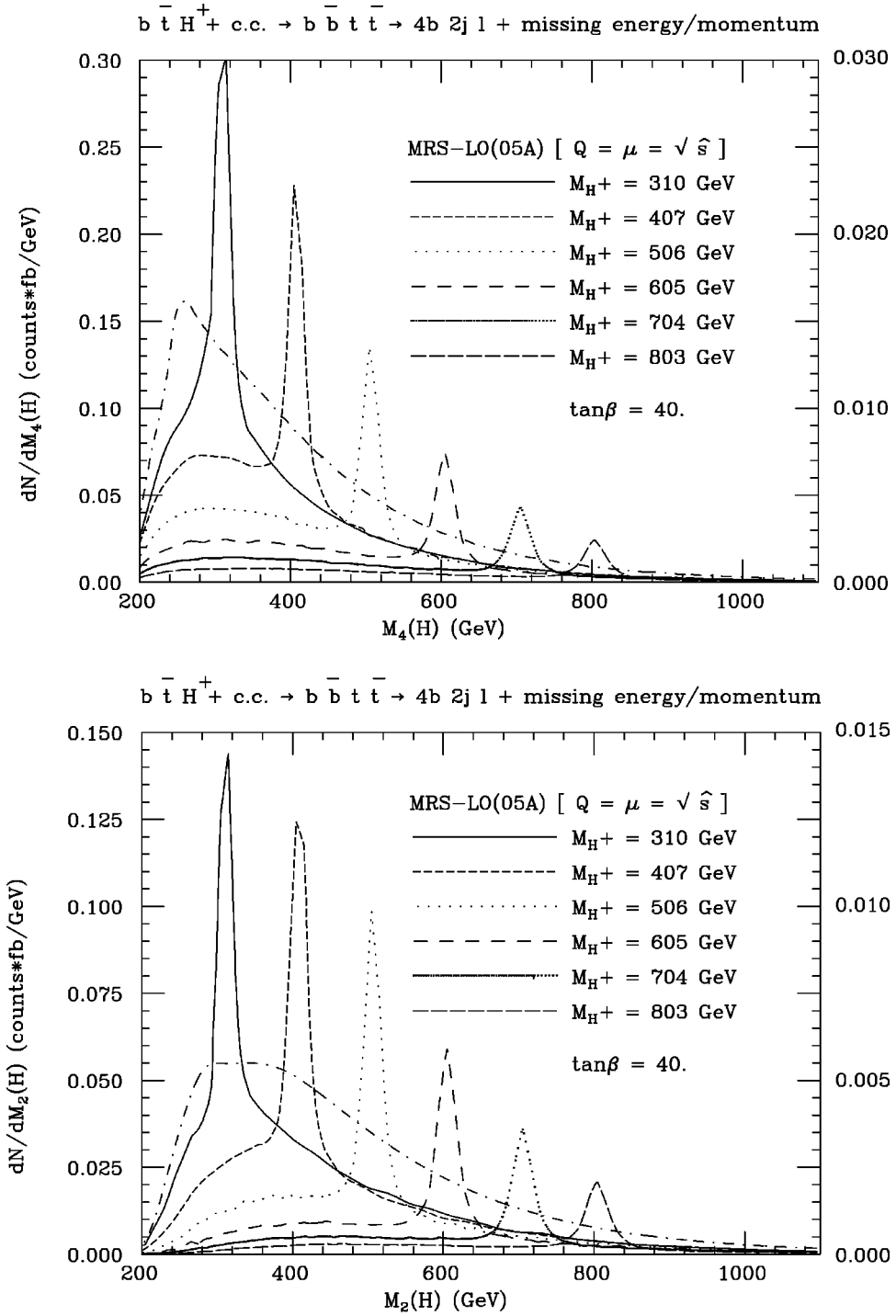

FIG. 4. Differential distributions in the reconstructed charged Higgs boson mass for process (4) (and its charge conjugate) in the decay channel (31) for six selected values of $M_{H^\pm}$ in the heavy mass range, for $\tan\beta=40$. Acceptance and selection cuts have been implemented here, along with the additional cuts (39) on the $2b$ system accompanying the $t\bar{t}$ pair. The PDF set used was MRS-LO(05A) with renormalization and factorization scales set equal to the partonic c.m. energy. The seventh (dot-dashed) curve represents the shape of the background (5) yielding the same signature (31). Normalization is to the total cross sections times the number of possible ''$2b+2$ jet mass'' combinations: four (top) and two (bottom). The right-hand scale corresponds to a b-tagging efficiency factor of $\epsilon_b^4=0.1$, i.e., $\epsilon_b=56\%$.

However, given the not too large rates of the surviving Higgs events, the actual size of the MSSM parameter space that can be covered strongly depends on the b-tagging efficiency c_b. For instance, changing it from 56% to 40% would result in a reduction of ϵ_b^4 by a factor of 4. This corresponds to a suppression of the $S/\sqrt{B}$ rates of Table IV by a factor of 2. A similar effect would occur if a 30 GeV cut in transverse momenta of both missing and observable particles is enforced, as opposed to the 20 GeV value advocated here. In this case, the suppression would be somewhat smaller though, about a factor of 3 on the event rates and 1.7 on the statistical significances.

Before concluding, we would like to come back to and justify what we have mentioned in the Introduction: that the size of the backgrounds (6),(7) is generally smaller than that of process (5) considered so far, for the b-tagging efficiencies assumed in this paper. Rather than rerunning all the simulations for each of these additional final states, we have assumed the two (anti) top quarks to have already been reconstructed, with similar efficiency in each case. This way, we can compute the $2\rightarrow4$ cross sections (6),(7) and apply the transverse momentum, pseudorapidity, and separation cuts of Sec. III to the jet-jet system accompanying the $t\bar{t}$ pair, alongside those of Eq. (39). We do so also for the case of process

TABLE IV. Number of events from signal (4) (and its charge conjugate) *(S)* and background (5) (*B*) in the decay channel (31), along with the statistical significance ($S/\sqrt{B}$), per 100 inverse femtobarns of integrated luminosity, in a window of 80 GeV around a few selected values of $M_{H^\pm}$ (given in GeV) in the heavy mass range, with $\tan\beta=40$. Four *b* jets are assumed to be tagged with overall efficiency $\epsilon_b^4=0.1$, i.e., $\epsilon_b=56\%$. All cuts discussed in the text, (32)–(35), (a)–(d) and (39), have been implemented. The renormalization and factorization scales are set equal to the partonic c.m. energy. The first row corresponds to the $M_4(H)$ distribution, whereas the second refers to the $M_2(H)$ one (see Fig. 4).

	Number of events per year		
$M_{H^\pm}\pm 40$ GeV	S	B	$S/\sqrt{B}$
310	127.80	105.14	12.46
	57.80	41.90	8.92
407	88.56	67.63	10.76
	53.78	39.21	8.58
506	51.46	38.74	8.26
	36.32	26.86	7.00
605	29.43	21.49	6.34
	22.70	16.58	5.57
704	17.09	11.98	4.93
	14.02	9.89	4.45
803	10.03	6.75	3.86
	8.61	5.81	3.57
	MRS-LO $[Q=\mu=\sqrt{\hat{s}}]$		
$4b+2$ jets$+l^\pm+p_{\rm miss}^T$			After all cuts

(5). (For all such computations we have resorted again to MADGRAPH [25].) By adopting $\epsilon_b=0.56$ and assuming $\epsilon_{g,q\neq b}=0.01$ to be the rejection factor against non-*b* jets, then the rates obtained this way scale as follows:

$$\sigma(gg\to t\bar{t}b\bar{b}):\sigma(gb\to t\bar{t}gb):\sigma(gg\to t\bar{t}gg+t\bar{t}q\bar{q}) \approx 3.38:0.56:0.48. \quad (40)$$

Thus, the singly and doubly *b* mistagged backgrounds are both one order of magnitude smaller than the pure $4b$ process. The same applies also to the other channel contributing to a possible double *b* mistagging, i.e.,

$$gq\to t\bar{t}gq, \quad (41)$$

where $q\neq b$, whose production rates are in fact comparable to those of process (5) (about 25% smaller). Altogether, they would add a 40% or so contribution to the $t\bar{t}b\bar{b}$ background. Some of these backgrounds are likely to be enhanced by a larger probability of a *c*-quark jet faking a *b* tag, which we have not taken into account. However, their inclusion would not change our main results, so that we have left these reactions aside for the time being.

V. SUMMARY AND CONCLUSIONS

The discovery at the LHC of charged scalar particles would definitely confirm the existence of new physics beyond the SM. In this respect, a very special role is played by the charged Higgs bosons of two-Higgs-doublet models (2HDMs), as their production and decay dynamics can entirely be described at the tree level by only two parameters. However, the feasibility of their detection at the LHC has always been far from certain if the mass of the new particles is much larger than the quark mass. Therefore, a high-on-the-list priority is to devise phenomenological strategies that would allow one to meet the difficult challenge of their detection at the LHC collider.

We have contributed here to this task by considering the production and decay of charged Higgs scalars of the MSSM in the channel $gg\to t\bar{b}H^-+t\bar{b}H^+\to b\bar{b}t\bar{t}\to b\bar{b}b\bar{b}W^+W^-$, in which one $W^\pm$ decays hadronically and the other leptonically. The major feature of our analysis, as compared to others carried out in the past, is that all four *b* quarks present in the final state are required to be recognized as such. The advantage of this procedure is that it allows one to exploit the differences existing between signal and background in the kinematics of the heavy quark jets. In fact, in the dominant background, $gg\to t\bar{t}b\bar{b}$, the two *b* quarks produced in association with the $t\bar{t}$ pair are soft, collinear, and at rather low invariant mass. In contrast, in the Higgs signal, at least one of the two is expected to be energetic and isolated, as long as $M_{H^\pm}$ is significantly larger than m_t. The disadvantage is that the additional *b* quark produced in Higgs events has rather low transverse momentum, so that its detection imposes a sizable loss of signal.

By exploiting a selection procedure that allows one to reconstruct both top quark and top antiquark masses and after imposing tight constraints on the two *b* quarks accompanying the $t\bar{t}$ pair, we do see Higgs peaks appearing on top of a flat combinatorial background and also above the continuum from $t\bar{t}b\bar{b}$ events. Their statistical significance is such that viable signals can be obtained for charged Higgs boson masses up to 600 GeV or so, when $\tan\beta$ is either below 1.5 or above 40, with a total number of Higgs events of the order of a several tens every 100 inverse femtobarns of luminosity.

Such mass coverage is significantly higher than that achieved in previous analyses based on a triple *b* tagging. However, we should stress that these conclusions rely on a high, though not unrealistic, *b*-tagging efficiency, of about 50% per single *b* jet, and a transverse momentum cut on jets and leptons, of 20 GeV, somewhat lower than the threshold normally considered. If such performances can be achieved by the LHC detectors while the machine is running at high luminosity, then the ''lepton plus $4b$'' channel represents a profitable new means to access such elusive yet crucial particles over significant portions of the MSSM parameter space. Besides, this channel will be very useful for the measurement of the charged Higgs boson parameters, given the higher purity of the signal in this case. Certainly, our results are sufficiently optimistic to justify a more detailed detector-level study, incorporating hadronization of the final state partons, and the effects of jet identification and reconstruction, as well as a full background simulation.

ACKNOWLEDGMENTS

D.J.M., S.M., and D.P.R. would like to thank the Centre for Particle Theory and Gray College at Durham University for the kind hospitality while part of this work was carried out. D.J.M. and S.M. are grateful to the UK-PPARC for research grants. D.P.R. thanks the UK-PPARC and IFCPAR for financial support. The authors are indebted to K. Odagiri for numerical comparisons and many fruitful discussions.

[1] J. F. Gunion, H. E. Haber, G. L. Kane, and S. Dawson, *The Higgs Hunters' Guide* (Addison-Wesley, Reading, MA, 1990).
[2] ALEPH Collaboration, R. Barate *et al.*, Report No. CERN/EP-99-011; L3 Collaboration, M. Acciarri *et al.*, Phys. Lett. B **446**, 368 (1999).
[3] ALEPH Collaboration, R. Barate *et al.*, Phys. Lett. B **440**, 419 (1998).
[4] M. Drees, E. Ma, P. N. Pandita, D. P. Roy, and S. K. Vempati, Phys. Lett. B **433**, 346 (1998).
[5] V. Barger, M. S. Berger, and P. Ohmann, Phys. Rev. D **47**, 1093 (1993).
[6] S. Moretti and W. J. Stirling, Phys. Lett. B **347**, 291 (1995); **366**, 451(E) (1996); A. Djouadi, J. Kalinowski, and P. M. Zerwas, Z. Phys. C **70**, 435 (1996); E. Ma, D. P. Roy, and J. Wudka, Phys. Rev. Lett. **80**, 1162 (1998).
[7] CDF Collaboration, F. Abe *et al.*, Phys. Rev. Lett. **79**, 357 (1997); M. Guchait and D. P. Roy, Phys. Rev. D **55**, 7263 (1997); E. Keith, E. Ma, and D. P. Roy, *ibid.* **56**, 5306 (1997).
[8] B. K. Bullock, K. Hagiwara, and A. D. Martin, Nucl. Phys. **B395**, 499 (1993).
[9] S. Raychaudhuri and D. P. Roy, Phys. Rev. D **52**, 1556 (1995); **53**, 4902 (1996).
[10] CMS Technical Proposal, Report No. CERN/LHCC/94-38, 1994; ATLAS Technical Proposal, Report No. CERN/LHCC/94-43, 1994.
[11] K. Odagiri, Phys. Lett. B **452**, 327 (1999).
[12] K. Odagiri, Report No. RAL-TR-1999-012, 1999, hep-ph/9901432; D. P. Roy, Phys. Lett. B **459**, 607 (1999).
[13] S. Moretti and K. Odagiri (in preparation).
[14] V. Barger, R. J. N. Phillips, and D. P. Roy, Phys. Lett. B **324**, 236 (1994).
[15] J. F. Gunion, Phys. Lett. B **322**, 125 (1994).
[16] A. A. Barrientos Bendezú and B. A. Kniehl, Phys. Rev. D **59**, 015009 (1999).
[17] S. Moretti and K. Odagiri, Phys. Rev. D **59**, 055008 (1999).
[18] S. Moretti and K. Odagiri, Phys. Rev. D **55**, 5627 (1997).
[19] J. L. Diaz-Cruz and O. A. Sampayo, Phys. Rev. D **50**, 6820 (1994).
[20] R. Kleiss and W. J. Stirling, Nucl. Phys. **B262**, 235 (1985).
[21] F. A. Berends, P. H. Daverveldt, and R. Kleiss, Nucl. Phys. **B253**, 441 (1985).
[22] C. Mana and M. Martinez, Nucl. Phys. **B287**, 601 (1987).
[23] S. Moretti, Phys. Rev. D **50**, 2016 (1994).
[24] E. Murayama, I. Watanabe, and K. Hagiwara, HELAS: HELicity Amplitude Subroutines for Feynman Diagram Evaluations, KEK Report No. 91-11, 1992.
[25] T. Stelzer and W. F. Long, Comput. Phys. Commun. **81**, 357 (1994).
[26] G. P. Lepage, J. Comput. Phys. **27**, 192 (1978).
[27] R. Kleiss, W. J. Stirling, and S. D. Ellis, Comput. Phys. Commun. **40**, 359 (1986).
[28] A. D. Martin, R. G. Roberts, W. J. Stirling, and R. S. Thorne, Phys. Lett. B **443**, 301 (1998).
[29] M. Spira, Report No. DESY 98-159, 1998, hep-ph/9810289; D. Dicus, T. Stelzer, Z. Sullivan, and S. Willenbrock, Phys. Rev. D **59**, 094016 (1999); F. Borzumati, J.-L. Kneur, and N. Polonsky, *ibid.* **60**, 115011 (1999).
[30] A. Djouadi, J. Kalinowski, and M. Spira, Comput. Phys. Commun. **108**, 56 (1998).
[31] J. A. Coarasa, D. Garcia, J. Guasch, R. A. Jiménez, and J. Solà, Phys. Lett. B **425**, 329 (1998).
[32] ATLAS Collaboration, E. Richter-Was and M. Sapinski, internal note ATL-PHYS-98-132; CMS Collaboration, V. Drollinger, T. Muller, and R. Kinnunen, internal note CMS NOTE 1999/001.
[33] G. P. Yeh (private communication).